938–941 (1972).
17. Aspect, A., Grangier, P. & Roger, G. Experimental realization of Einstein-Podolsky-Rosen-Bohm gedanken experiment: A new violation of Bell's inequalities. *Phys. Rev. Lett.* **49,** 91–94 (1982).
18. Ou, Z. Y. & Mandel, L. Violation of Bell's inequality and classical probability in a two-photon correlation experiment. *Phys. Rev. Lett.* **61,** 50–53 (1988).
19. Tittel, W., Brendel, J., Zbinden, H. & Gisin, N. Violation of Bell inequalities by photons more than 10 km apart. *Phys. Rev. Lett.* **81,** 3563–3566 (1998).
20. Weihs, G., Jennewein, T., Simon, C., Weinfurter, H. & Zeilinger, A. Violation of Bell's inequality under strict Einstein locality conditions. *Phys. Rev. Lett.* **81,** 5039–5043 (1998).
21. Sakurai, J. J. *Modern Quantum Mechanics* 203 (Addison-Wesley, Reading, Massachusetts, 1994).
22. Aspect, A. in *The Wave-Particle Dualism* (eds Diner, S., Farque, D., Lochak, G. & Selleri, F.) 377 (D. Reidel Publishing Company, Dordrecht, 1984).
23. Kroupa, G. *et al.* Basic features of the upgraded S18 neutron interferometer set-up at ILL. *Nucl. Instrum. Meth. A* **440,** 604–608 (2000).
24. Rauch, H., Wilfing, A., Bauspiess, W. & Bonse, U. Precise determination of the 4 pi-periodicity factor of a spinor wave function. *Z. Phys. B* **29,** 281–284 (1978).
25. Michler, M., Weinfurter, H. & Zukowski, M. Experiments towards falsification of noncontextual hidden variable theories. *Phys. Rev. Lett.* **84,** 5457–5461 (2000).
26. Englert, B.-G. Remark on some basic issues in quantum mechanics. *Z. Naturforsch.* **54a,** 11–32 (1999).
27. Bell, J. S. in *Themes in Contemporary Physics II* (eds Deser, S. & Finkelstein, R. J.) 1 (World Scientific, Singapore, 1989).

Acknowledgements We appreciate discussions with R. A. Bertlmann, I. J. Cirac and D. Home. This work has been supported by the Austrian Fonds zur Föderung der Wissenschaftlichen Forschung.

Competing interests statement The authors declare that they have no competing financial interests.

Correspondence and requests for materials should be addressed to Y.H. (hasegawa@ati.ac.at).

Entangled quantum state of magnetic dipoles

S. Ghosh[1], T. F. Rosenbaum[1], G. Aeppli[2] & S. N. Coppersmith[3]

[1]*James Franck Institute and Department of Physics, University of Chicago, Chicago, Illinois 60637, USA*
[2]*London Centre for Nanotechnology and Department of Physics and Astronomy, University College London, London WC1E 6BT, UK, and NEC Laboratories, 4 Independence Way, Princeton, New Jersey 08540, USA*
[3]*Department of Physics, University of Wisconsin, Madison, Wisconsin 53706, USA*

Free magnetic moments usually manifest themselves in Curie laws, where weak external magnetic fields produce magnetizations that vary as the reciprocal of the temperature ($1/T$). For a variety of materials that do not display static magnetism, including doped semiconductors[1] and certain rare-earth intermetallics[2], the $1/T$ law is replaced by a power law $T^{-\alpha}$ with $\alpha < 1$. Here we show that a much simpler material system—namely, the insulating magnetic salt $LiHo_xY_{1-x}F_4$—can also display such a power law. Moreover, by comparing the results of numerical simulations of this system with susceptibility and specific-heat data[3], we show that both energy-level splitting and quantum entanglement are crucial to describing its behaviour. The second of these quantum mechanical effects—entanglement, where the wavefunction of a system with several degrees of freedom cannot be written as a product of wavefunctions for each degree of freedom—becomes visible for remarkably small tunnelling terms, and is activated well before tunnelling has visible effects on the spectrum. This finding is significant because it shows that entanglement, rather than energy-level redistribution, can underlie the magnetic behaviour of a simple insulating quantum spin system.

The insulator that we focus on in the search for the cause of the anomalous power-law divergence of the magnetic susceptibility is $LiHo_xY_{1-x}F_4$, a salt where magnetic Ho^{3+} ions are randomly substituted for nonmagnetic Y^{3+} with probability x. For $x = 1$, the material is the dipolar-coupled ferromagnet, $LiHoF_4$, with a Curie temperature of 1.53 K. Randomly distributing dipoles in a solid matrix provides quenched disorder, while the angular anisotropy of the dipole–dipole interaction leads to competition between ferromagnetic and antiferromagnetic bonds and the possibility of many (nearly) degenerate ground states[4]. Indeed, the low-temperature magnetic phase diagram of the dipolar-coupled rare-earth tetrafluorides progresses smoothly from long-range order to glassiness with increasing spin dilution[3]. What interests us here, however, is the considerably diluted $x = 0.045$ compound, where we have observed[5,6]—contrary to classical expectations[4]—novel 'antiglass' behaviour as well as long-lived spin oscillations whose qualitative understanding seems to require mesoscopic quantum coherence. We show in Fig. 1 the experimental d.c. susceptibility, χ, plotted against temperature, T, for a single-crystal specimen of the material. What emerges is not the standard Curie law, $1/T$, expected for non-interacting magnetic moments, but instead a diverging response following a power law $T^{-\alpha}$, with $\alpha = 0.75 \pm 0.01$. This power law is close to that associated with the diverging local susceptibilities inferred for doped silicon[1] as well as metallic rare-earth materials[2] on the brink of magnetic order. What is most striking, however, is that the magnetic susceptibility for $LiHo_{0.045}Y_{0.955}F_4$ is a smoothly diverging quantity, even though the magnetic specific heat (C, Fig. 2a) is characterized by unusually sharp peaks in the same temperature range. In ordinary materials containing magnetic ions, there is a strong correlation between magnetic susceptibility and specific heat in the sense that anomalies, especially as strong as the

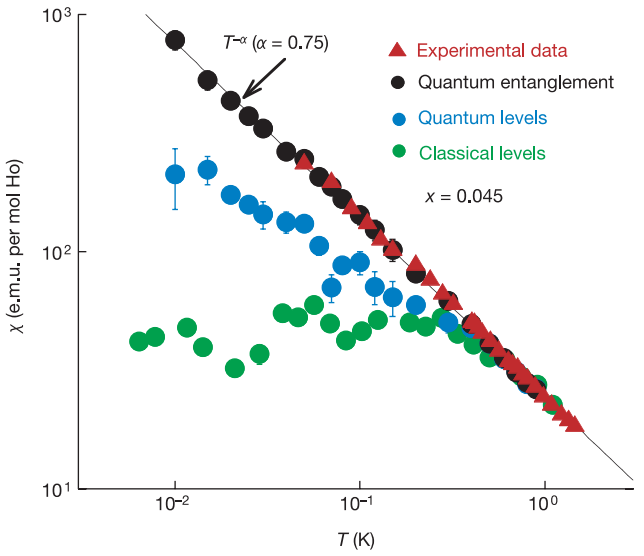

Figure 1 Magnetic susceptibility χ versus temperature T of the diluted, dipolar-coupled Ising magnet, $LiHo_{0.045}Y_{0.955}F_4$. Red triangles, experimental data; filled circles, simulations. Green circles, classical decimation when the calculations are performed with $g_\perp = 0$. Blue circles, susceptibility computed using the classical procedure, equation (3), of determining Curie constants by adding (subtracting) moments when the ground state is predominantly ferromagnetic (antiferromagnetic), but with quantum decimation, using energy levels derived from the full dipolar hamiltonian of equation (1). Although the susceptibility approaches that of the experiment more closely than before, it still deviates by at least a factor of four at low temperatures. Black circles, use of quantum decimation as well as the correct quantum mechanical form of susceptibility given by equation (5), using the entanglement of the low-lying energy doublet with the excited states. The line is a best fit to $\chi(T) \propto T^{-\alpha}$, with $\alpha = 0.75 \pm 0.01$. Although α is always less than 1, it is not a universal number. It varies from 0.62 to 0.81 as the concentration x decreases from 0.1 to 0.01, a trend also observed in Heisenberg systems[7]. The simulation results have not been scaled, and agree quantitatively with the experimental results.

sharp peaks in the specific heat, are reflected in the susceptibility.

The data for $LiHo_{0.045}Y_{0.955}F_4$ thus provide three puzzles: the absence of a spin glass transition predicted for a collection of randomly placed dipoles, the anomalous power-law behaviour $\chi \propto T^{-\alpha}$, and the coexistence of a featureless power law in χ with sharp anomalies in the specific heat. We show here that it is an intrinsic quantum mechanical term in the dipole hamiltonian that stabilizes the spin liquid 'antiglass' and resolves the puzzles. Following a pair-wise 'decimation' procedure[7–13] adapted to treat the full axial and transverse components of the dipole–dipole interaction, we find that quantum fluctuations continue to provide channels for relaxation down to the lowest temperatures. We simulate the evolution with temperature T of both the magnetic susceptibility and the heat capacity using the actual interaction parameters between Ho moments obtained from various experimental results, and compare quantitatively the results of simulation and experiment.

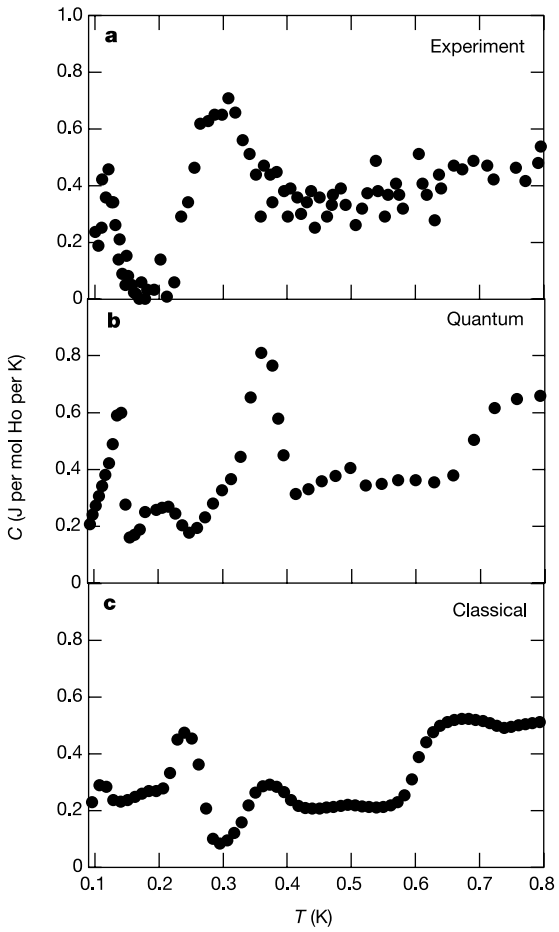

Figure 2 Comparison of the temperature-dependent experimental electronic specific heat $C(T)$ for $LiHo_{0.045}Y_{0.955}F_4$ with different simulation techniques. **a**, Experimental data showing two sharp Schottky-like features dominating the thermal response. **b**, Quantum decimation, emphasizing how the well-defined energy levels result in a more complex temperature-dependent specific heat with greater resemblance to the experimental data, especially at low temperatures. Notably, there is the appearance of a sharp peak at 130 mK, close to a similar feature in the data. **c**, Classical decimation, demonstrating some success in calculating $C(T)$ but with the characteristic sharp features occurring at incorrect temperatures. The features occur as k_BT moves through maxima in the distribution of dipolar couplings, and are affected as the concentration x varies; this distribution is granular, because the dipolar interaction is being sampled between points on a lattice rather than in continuous space.

$LiHoF_4$ crystallizes in a body-centred tetragonal ($CaWO_4$) structure with lattice constants[14] $a = a' = 5.175(5)$ Å and $c = 10.75(1)$ Å. Each unit cell has four formula units with the magnetic Ho^{3+} ions occupying positions (0, 0, 0), (0, a/2, c/4), (a/2, a/2, c/2) and (a/2, 0, 3c/4). The Ising axis is defined by the crystal field of the Ho^{3+} ions that forces the spin-1/2 magnetic moments with a g-factor of 13.8 to point along the crystalline c axis. We generate a model of the three-dimensional lattice of $LiHo_xY_{1-x}F_4$ on the computer by repeated translation of the unit cell vectors. N spins are distributed randomly in this lattice with probability of occupancy x on the body-centred tetragonal sites. Periodic boundary conditions are applied. We have used a maximum of $N = 400$ spins (8×10^4 pair-wise interactions), and have checked that our results are in the N-independent limit. The Ising spin (σ_i^z) at each site i is assigned a value of 1 or -1 randomly. We have confirmed explicitly that in the dilute limit of x the outcome is not sensitive to this particular initial condition, obviating the need to average over initial spin configurations. Our simulations incorporate pair-wise dipolar couplings, in which the interaction energy between two magnetic dipole moments $\mathbf{M}_1$ and $\mathbf{M}_2$ separated by the vector $\mathbf{r} = \hat{\mathbf{r}}r$ is

$$E_{\text{int}} = \frac{1}{r^3}(\mathbf{M}_1 \cdot \mathbf{M}_2 - 3(\hat{\mathbf{r}} \cdot \mathbf{M}_1)(\hat{\mathbf{r}} \cdot \mathbf{M}_2)) \quad (1)$$

The magnetic dipole moment $\mathbf{M}_i$ at site i is related to the spin $\boldsymbol{\sigma}_i$ via $M_{i\lambda} = \mu_i g_\lambda \sigma_{i\lambda}$ ($\lambda = x, y, z$) where μ_i is the magnetic moment of the ith spin, initially $\mu_i = \mu_B/2$ for all i, and the elements of the anisotropic g-factor matrix ($g_x = g_y = g_\perp = 0.74$, $g_z = g_\parallel = 13.8$) are known from previous measurements on the pure material[14–16].

Our first simulation is a classical calculation in which $g_\perp = 0$ and equation (1) reduces to $-2M_{1z}M_{2z}/r^3$. The hamiltonian can be

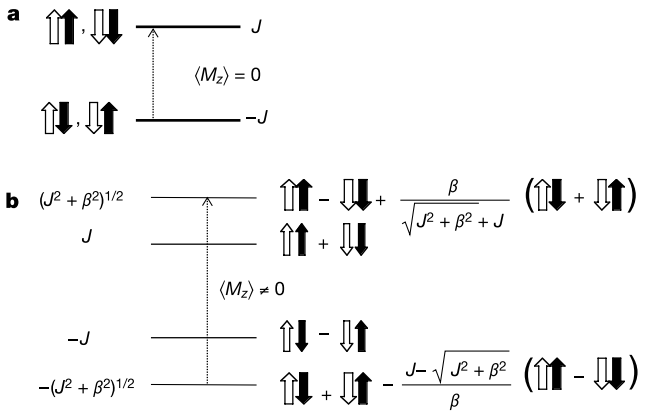

Figure 3 Diagram detailing the difference between the classical and the quantum decimation schemes. **a**, The classical energy levels calculated using equation (2). There are two doubly degenerate energy levels, designated $+J$ and $-J$. Depending on the value of the angle formed by the Ising axis and the vector connecting the spins, the ground state $-J$ can correspond to antiferromagnetic or ferromagnetic alignment of (i,j). The eigenstates commute with σ_z, and there is no mixing between the ground-state doublet and the excited states. **b**, The quantum energy levels, showing the new entangled eigenstates. β is the off-diagonal term of the full dipolar interaction of equation (1), which reduces to the well-known hamiltonian of Ising spins in a transverse magnetic field in the limit of small $(g_\perp/g_\parallel)^2$. The two doublets are split to produce eigenstates that are mixtures of the classical states. It is not only states from the same doublet that are mixed: β also yields a ground state that mixes ferromagnetic and antiferromagnetic classical states. Thus, the off-diagonal terms in the dipolar interaction introduce both a change in the spectrum (in the form of splittings of the doublets as well as shifts of the 'ferromagnetic' excited states relative to the 'antiferromagnetic' ground state), and mixing (or 'entanglement') of the classical states.

written as:

$$H = -\sum_{i,j}^{N} J_{ij}\mu_i\sigma_{iz}\mu_j\sigma_{jz} \quad (2)$$

where J_{ij} (which assimilates the numerical constants and the product $g_{\parallel}^2$) falls off as $1/r^3$ and the quantities denoted by σ are classical Ising spins that can take the values ± 1. It is expected to be valid both in the very dense ($x = 1$) ferromagnetic and very dilute ($x \to 0$) paramagnetic limits. We call equation (2) an 'axial dipole' hamiltonian, as the dipolar field of spin j coupling to the moment of spin i acts only along the Ising axis. We show in Fig. 3a the energy levels calculated using equation (2) for a spin pair (i,j) when $|\mu_i| = |\mu_j|$.

Once we have calculated the energy of all spin pairs, we arrange the pairs in a hierarchy based on their coupling strength and pick the pair with the largest energy $|J_{max}|$. If $2|J_{max}| > k_BT$, the excited state $+J_{max}$ becomes redundant and this pair is forced into its ground state. The pair is replaced by a composite single spin of equivalent net magnetic moment that can be either $\mu_C = |\mu_i| - |\mu_j|$ (antiferromagnetic interaction) or $\mu_C = |\mu_i| + |\mu_j|$ (ferromagnetic interaction). If the net moment is zero, the two spins are 'decimated' (that is, eliminated) and removed from further consideration; otherwise they are replaced by one spin with the new composite moment placed at the average position of the two spins in the pair. Only the magnetic moment μ_C and the position $\mathbf{r}_C$ of the pair are renormalized; $g_{\parallel}$ is left unchanged. The new magnetic dipole moment M_{Cz} is now given by $\mu_C g_{\parallel}\sigma_{Cz}$ ($M_{Cx} = M_{Cy} = 0$). The altered demography requires the procedure to begin anew with the calculations of the pair-wise interactions between the remaining spins and the composite $\mathbf{M}_C$ at $\mathbf{r}_C$ using equation (2). At each iteration one spin pair is either eliminated or transformed into a single spin degree of freedom until the strongest pair remaining has a gap $2|J_{max}| < k_BT$. All spins remaining in the system are considered 'free' at that T. We choose $T = 1$ K at the outset, given that the nearest-neighbour interaction energy $J_{nn} = 1.2$ K; the temperature is then lowered in steps $\Delta T = 0.01$ K down to $T = 0.01$ K.

At each temperature, the calculation produces a list $\{M_i\}$ of $N(T)$ 'free' moments. Given that the susceptibility for a free Ising moment M_i is M_i^2/k_BT and its contribution to the entropy is $(R\ln 2)N(T)$, we can compute the specific heat and susceptibility via the relations:

$$\chi = \sum_i \frac{M_i^2}{k_BT} \quad (3)$$

and

$$C = \frac{T\mathrm{d}S}{\mathrm{d}T} = RT\ln 2\frac{\mathrm{d}N(T)}{\mathrm{d}T} \quad (4)$$

Figure 2c reveals one success of the classical decimation approach, namely the appearance of sharp features in the specific heat. Although the features are of roughly the same magnitude as seen in the experiment, they do not occur at the correct temperatures. Figure 1, where the filled green circles are the results of the classical calculation, reveals a more disturbing problem. In accord with intuition, but in disagreement with experiment, there are sharp anomalies in χ that coincide with the peaks in C. Moreover, the classical susceptibility at low temperatures is over an order of magnitude smaller than that measured.

The axial dipole hamiltonian in equation (2) takes into account only the interactions parallel to the Ising axis by ignoring $g_{\perp}$ and treats the spins as classical bits rather than Pauli matrices. For pure $LiHoF_4$ in its ferromagnetic state, this is the complete picture, because the lattice symmetry ensures that at any site the perpendicular component of the dipolar field due to the other spins sums to zero. However, as the magnetic Ho^{3+} ions are randomly replaced by non-magnetic Y^{3+}, all transverse components are no longer perfectly compensated, and at dipole concentrations of only a few per cent the site-specific, internal transverse fields can be as large as 1 kOe. With a finite $g_{\perp}$, the full hamiltonian, equation (1), no longer reduces to equation (2), but acquires off-diagonal terms of the form $\beta\sigma_{ix}\sigma_{jz}$, where β includes numerical constants and the product $g_{\perp}g_{\parallel}$. Terms of order $\sigma_{ix}\sigma_{jx}$ are not included, because $g_{\perp}^2 \ll g_{\perp}g_{\parallel} \ll g_{\parallel}^2$.

The results in Figs 1 and 2 demonstrate how the decimation calculation is affected when the energy levels but not the eigenfunctions are modified to account for the inclusion of the off-diagonal terms of the dipolar interaction. Although the basic decimation scheme remains the same, there are now two energy scales available for comparison with temperature: $2|J|$ and $(J^2 + \beta^2)^{1/2} - J$, which is $\sim\beta^2/2J$ to first order. As this second gap is much smaller than the first, it becomes clear that, at a temperature T, the number of free spins, $N(T)$, is greater than in the classical case (see Fig. 3b). The results of this modification meet with partial success. The increase in $N(T)$ can account better for the specific-heat characteristics (Fig. 2b), but not for the susceptibility, especially at low temperatures (Fig. 1, filled green circles), implying that it is not merely the excess in the number of free spins that enhances and smoothes the susceptibility of the sample.

The key to matching the experimental susceptibility result is to use the quantum mechanical expression[17] for χ:

$$\chi = \sum_i^N \frac{1}{\sum_n \rho_n(i)} \sum_n \left(\frac{\left(E_n^{(1)}(i)\right)^2}{k_BT} - 2E_n^{(2)}(i) \right) \rho_n(i) \quad (5)$$

with

$$\rho_n(i) = \exp\left(\frac{-E_n^{(0)}(i)}{k_BT}\right); \quad E_n^{(1)}(i) = \langle n(i)|M_{iz}|n(i)\rangle \text{ and}$$

$$E_n^{(2)}(i) = \sum_m \frac{|\langle n(i)|M_{iz}|m(i)\rangle|^2}{E_m^{(0)}(i) - E_n^{(0)}(i)}$$

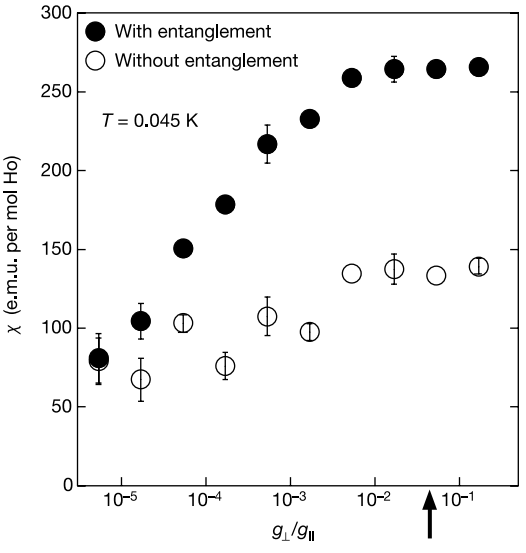

Figure 4 The change in susceptibility as the quantum entanglement is tuned by varying the ratio of the transverse and longitudinal magnetic g-factors, $g_{\perp}/g_{\parallel}$. An arrow denotes the value for $LiHo_{0045}Y_{0.955}F_4$. The full quantum susceptibility (filled circles) demonstrates extraordinary sensitivity to the slightest entanglement of the wavefunctions ($g_{\perp}/g_{\parallel} \approx 10^{-4}$), whereas the susceptibility calculated using the quantum energy levels but ignoring the entanglement (open circles) is relatively flat. Quantum entanglement produced by the off-diagonal terms, rather than spectral superposition, dominates the physics.

where first we sum over the energy levels of the ith effective spin remaining, and then sum over all N effective spins. Except for a population of isolated, unrenormalized spins that dwindles as T decreases, $|n\rangle$ and $|m\rangle$ are now the entangled pair eigenstates illustrated in Fig. 3b. Note that keeping only the first term in the brackets reduces equation (5) to equation (3). The result obtained using equation (5) (Fig. 1, black circles) agrees quantitatively with the actual measurements (Fig. 1, red triangles) of the magnetic susceptibility in the d.c. limit for $LiHo_{0.045}Y_{0.955}F_4$.

The inclusion of the off-diagonal terms, $E_n^{(2)}$, produces the reconciliation between simulation and experiment by superposing the antiferromagnetic ground state with the ferromagnetic excited state (Fig. 3b). In this manner, the excited classical states 'frozen out' by the decimation still enter into the expression for the susceptibility, thereby enhancing its value. The concurrence[18,19], which ranges from 0 (disentangled states) to 1 (completely entangled), quantifies entanglement in an exact way for bipartite systems. We identify the T-dependent entanglement τ as the concurrence of the pair wavefunctions contributing to the susceptibility at each T, weighted by the fraction of actual spins involved in the history of the pair formation within the decimation calculation. We find that $\tau = 0.11$ at 0.8 K, growing to 0.88 at 0.01 K, in accord with the trend from near agreement of the 'entangled' and 'quantum level' bulk susceptibilities at 0.8 K towards a factor of four difference at 0.01 K. Moreover, we find that only the slightest degree of entanglement can have profound effects. We illustrate this in Fig. 4, which shows how the two calculations evolve with increasing $g_\perp$. The figure reveals that a $g_\perp/g_\parallel$ as small as 10^{-4} produces a large change in χ. The effects of the energy-level distribution are minimal by comparison.

Contrary to intuition and common experience, a dilute assembly of Ising dipoles does not freeze when cooled to millikelvin temperatures. The computer simulations presented here indicate that it is quantum mechanics—the internal magnetic fields transverse to the Ising axis inherent to the dipole–dipole interaction—that stabilizes the spin liquid. However, unlike conventional spin liquids, where the dynamics are dominated by a single gap to triplet excitations, the dilute dipoles form a state with a distribution of such gaps, especially well probed by the specific heat, which shows remarkable releases of entropy at certain well-defined temperatures. At the same time, the magnetic susceptibility increases smoothly with decreasing temperature, but at a rate slower than a Curie law[6]. The smoothness is in marked contrast to the highly structured heat capacity, and can only be understood if quantum mechanical mixing—the entanglement of classical ferromagnetic and antiferromagnetic contributions to the wavefunctions—is taken into account. There is a growing realization[20–22] that entanglement is a useful concept for understanding quantum magnets, thus unifying two rapidly evolving areas, quantum information theory and quantum magnetism. The discussions to date have focused on one-dimensional magnets and measures of entanglement with clear theoretical meaning but no simple experimental implementation. Our experiments and simulations illustrate how entanglement, rather than energy-level redistribution, can contribute significantly to the simplest of observables—the bulk susceptibility—in an easily stated model problem. □

Received 29 April; accepted 7 July 2003; doi:10.1038/nature01888.

1. Paalanen, M. A., Ruckenstein, A. E. & Thomas, G. A. Spins in Si:P close to the metal-insulator transition. *Phys. Rev. Lett.* **54,** 1295–1298 (1985).
2. Schröder, A. *et al.* Onset of antiferromagnetism in heavy-fermion metals. *Nature* **407,** 351–355 (2000).
3. Reich, D. H. *et al.* Dipolar magnets and glasses: Neutron scattering, dynamical, and calorimetric studies of randomly distributed Ising spins. *Phys. Rev. B* **42,** 4631–4644 (1990).
4. Aharony, A. & Stephen, M. J. Percolation with long-range interactions. *J. Phys. C* **14,** 1665–1670 (1981).
5. Reich, D. H., Rosenbaum, T. F. & Aeppli, G. Glassy relaxation without freezing in a random dipolar-coupled Ising magnet. *Phys. Rev. Lett.* **59,** 1969–1972 (1987).
6. Ghosh, S., Parthasarathy, R., Rosenbaum, T. F. & Aeppli, G. Coherent spin oscillations in a disordered magnet. *Science* **296,** 2195–2198 (2002).
7. Bhatt, R. N. & Lee, P. A. Scaling studies of highly disordered spin-1/2 antiferromagnetic systems. *Phys. Rev. Lett.* **48,** 344–347 (1982).
8. Ma, S. K., Dasgupta, C. & Hu, C. K. Random antiferromagnetic chain. *Phys. Rev. Lett.* **43,** 1434–1437 (1979).
9. Dasgupta, C. & Ma, S. K. Low temperature properties of the random Heisenberg antiferromagnetic chain. *Phys. Rev. B* **22,** 1305–1319 (1980).
10. Fisher, D. S. Random transverse field Ising spin chains. *Phys. Rev. Lett.* **69,** 534–537 (1992).
11. Fisher, D. S. Critical behaviour of random transverse-field Ising spin chains. *Phys. Rev. B* **51,** 6411–6461 (1995).
12. Westerberg, E., Furusaki, A., Sigrist, M. & Lee, P. A. Random quantum spin chains: A real space renormalization group study. *Phys. Rev. Lett.* **75,** 4302–4305 (1995).
13. Phillips, P., Izzo, D. & Kundu, K. Spin-lattice relaxation below 1 K: A new mechanism for unexpected nuclear spin relaxation. *Phys. Rev. B* **37,** 10876–10879 (1988).
14. Hansen, P. E., Johansson, T. & Nevald, R. Magnetic properties of lithium rare-earth fluorides: Ferromagnetism in $LiErF_4$ and $LiHoF_4$ and crystal-field parameters at the rare-earth and Li sites. *Phys. Rev. B* **12,** 5315–5324 (1975).
15. Bitko, D., Rosenbaum, T. F. & Aeppli, G. Quantum critical behaviour for a model magnet. *Phys. Rev. Lett.* **77,** 940–943 (1996).
16. Magarino, J., Tuchendler, J., Beauvillain, P. & Laursen, I. EPR experiment in $LiTbF_4$, $LiHoF_4$, and $LiErF_4$ at submillimeter frequencies. *Phys. Rev. B* **21,** 18–28 (1980).
17. Van Vleck, J. H. Quantum mechanics—the key to understanding magnetism. *Rev. Mod. Phys* **50,** 181–189 (1978).
18. Gunlycke, D., Kendon, V. M., Vedral, V. & Bose, S. Thermal concurrence mixing in a one-dimensional Ising model. *Phys. Rev. A* **64,** 042302 (2001).
19. Wootters, W. K. Entanglement of formation of an arbitrary state of two qubits. *Phys. Rev. Lett.* **80,** 2245–2248 (1998).
20. Osterloh, A., Amico, L., Falci, G. & Fazio, R. Scaling of entanglement close to a quantum phase transition. *Nature* **416,** 608–610 (2002).
21. Arnesen, M. C., Bose, S. & Vedral, V. Natural thermal and magnetic entanglement in the 1D Heisenberg model. *Phys. Rev. Lett.* **87,** 017901 (2001).
22. Osborne, T. J. & Nielsen, M. A. Entanglement, quantum phase transitions, and density matrix renormalization. *Quant. Inform. Process.* **1,** 45–53 (2002).

Acknowledgements We thank R. Parthasarathy for discussions. The work at the University of Chicago was supported by the MRSEC Program of the National Science Foundation, that in the University of Wisconsin by the Petroleum Research Fund and the National Science Foundation, and that in University College London by a Wolfson–Royal Society Research Merit Award and the Basic Technologies programme of the UK Research Councils.

Competing interests statement The authors declare that they have no competing financial interests.

Correspondence and requests for materials should be addressed to T.F.R (t-rosenbaum@uchicago.edu).

Magnetic enhancement of superconductivity from electron spin domains

H. A. Radovan[1], N. A. Fortune[2], T. P. Murphy[1], S. T. Hannahs[1], E. C. Palm[1], S. W. Tozer[1] & D. Hall[1]*

[1]*NHMFL, Florida State University, Tallahassee, Florida 32310, USA*
[2]*Department of Physics, Smith College, Northampton, Massachusetts 01063, USA*

* Present address: American Physical Society, One Research Road, Box 9000, Ridge, New York 11961, USA

Since the discovery of superconductivity[1], there has been a drive to understand the mechanisms by which it occurs. The BCS (Bardeen–Cooper–Schrieffer) model successfully treats the electrons in conventional superconductors as pairs coupled by phonons (vibrational modes of oscillation) moving through the material[2], but there is as yet no accepted model for high-transition-temperature, organic or 'heavy fermion' superconductivity. Experiments that reveal unusual properties of those superconductors could therefore point the way to a deeper understanding of the underlying physics. In particular, the response of a material to a magnetic field can be revealing, because this usually reduces or quenches superconductivity. Here we report measurements of the heat capacity and magnetization that show that, for particular orientations of an external